Interaction of delaminations and matrix cracks in a CFRP plate, Part I: A test method for model validation

Mark McElroy*,[1], Wade Jackson[1], Robin Olsson[2], Peter Hellström[2], Spyros Tsampas[2], Mark Pankow[3]

Abstract

Isolating and observing the damage mechanisms associated with low-velocity impact in composites using traditional experiments can be challenging, due to damage process complexity and high strain rates. In this work, a new test method is presented that provides a means to study, in detail, the interaction of common impact damage mechanisms, namely delamination, matrix cracking, and delamination-migration, in a context less challenging than a real impact event. Carbon fiber reinforced polymer specimens containing a thin insert in one region were loaded in a biaxial-bending state of deformation. As a result, three-dimensional damage processes, involving delaminations at no more than three different interfaces that interact with one another via transverse matrix cracks, were observed and documented using ultrasonic testing and x-ray computed tomography. The data generated by the test is intended for use in numerical model validation. Simulations of this test are included in Part II of this paper.

Keywords: A. Laminates, B. Delamination, C. Transverse cracking, D. Mechanical testing

*Corresponding author, mark.w.mcelroy@nasa.gov
[1]NASA Langley Research Center, 2 W. Reid St, Mail Stop 188E, Hampton, VA 23681
[2]Swerea SICOMP, Gothenburg, Sweden
[3]North Carolina State University, Raleigh, NC 27695

1. Introduction

Composite laminate materials in aerospace structures are inherently susceptible to damage from transverse loads, such as impact. This vulnerability necessitates a lengthy design and certification process to ensure structural reliability and safety. Currently there is a lack of robust and reliable damage simulation tools, and without such tools, certification of composite structures relies almost entirely on testing [1, 2]. If reliable damage simulation tools were available for composites, certain tests could be replaced with analysis and a cheaper and faster design process may be realized [3, 4, 5].

A challenge for developing numerical damage simulation tools for composites is obtaining validation data. Damage processes in laminates often occur quickly and are very complex, consisting of perhaps dozens of interacting delaminations and matrix cracks in a three-dimensional network. A common cause of this type of damage is low-velocity impact (LVI). Figure 1 is a section view of typical LVI damage in a laminate. The development of simulation models that can predict a complex three-dimensional network of cracks such as this, in a reliable manner, has had some success to date, but has proven to be difficult [6, 7]. Future model development and improvement relies in part on having access to useful validation data.

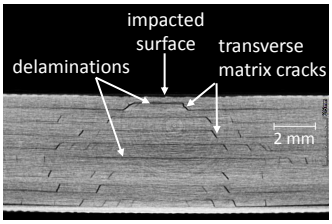

Figure 1: Typical low-velocity impact damage in a composite plate.

The approach commonly used when creating a new progressive damage simulation methodology is to start with validation of simple damage cases, such as standard delamination coupon models, and develop the method incrementally by increasing the complexity of the validation cases. In order to use this approach, experimental data are needed at each stage of development. Validation

data, which are often obtained from ASTM standard tests [8, 9, 10] using simple coupon-sized unidirectional laminate structures, are available from several sources (e.g., [11, 12]). Damage documented in these tests is confined to one ply interface and does not replicate the extensive damage that can result from LVI (see Figure 1).

A slightly more complex damage process may include transverse matrix cracking. In Ratcliffe et al.'s delamination-migration experiment, delamination grows from an implanted delamination starter, then migrates to a new interface via a transverse matrix crack, and then continues growth at that new interface [13]. This experiment is useful in progressive damage model development and validation, as it isolates a specific damage mechanism; however, it is designed to do only that, not to represent a more extensive damage scenario such as LVI, where dozens of delaminations may be occurring and interacting.

It is helpful to consider damage problems of medium complexity, in between that of the delamination-migration experiment and that of LVI. "Medium complexity" in this context may be defined as progressive damage in a laminate that involves no more than two or three delaminations at different interfaces, which interact via transverse matrix cracks. The goal of the research described in this paper is to generate medium complexity experimental data to be used in model development and validation, and also to gain further fundamental understanding of laminate damage processes associated with LVI. A new biaxial-bending test is developed to achieve this goal. Both quasi-static indentation and low-velocity impact loads are used in the tests. Following the introduction, in sequential order, this paper contains a description of the experiments, results and discussion pertaining to the quasi-static tests (Layups 1–3), results and discussion pertaining to the impact tests (Layups 1–3), a section on the specimen fracture surface microscopy, and conclusions.

2. Experiment description

2.1. Overview

An experiment was designed which creates a progressive damage process that consists of multiple delaminations growing at different interfaces and interacting with one another via transverse matrix cracks in a carbon fiber reinforced polymer (CFRP) specimen. The specimens, square in shape and containing a quarter-circle pre-existing delamination in one corner, were placed in a clamping test fixture such that only the two specimen edges opposite the pre-existing delamination were restrained. A load was applied to the corner of the specimen containing the pre-existing delamination. These loading and boundary conditions result in a biaxial-bending state of deformation in the specimen. The test is illustrated in Figure 2. Simulations of this test using an enriched shell element model are presented in Part II of this paper [14].

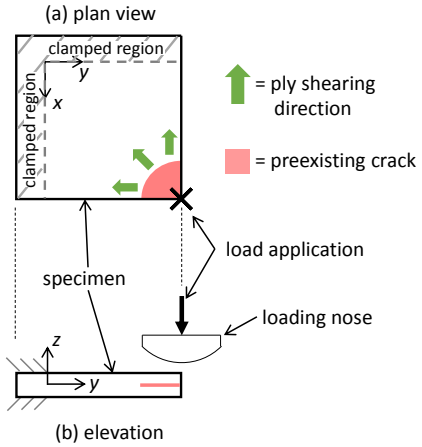

Figure 2: Test schematic.

Canturri et al. performed a test that was configured similarly [15], which served as inspiration for this test. The primary difference between Canturri et al.'s test and the test described herein is the biaxial-bending deformation. The biaxial-bending state, combined with the quarter circle geometry of the pre-existing delamination, results in a ply shearing direction (i.e., direction of maximum interlaminar shear stress) that varies radially in the specimen through

one full quadrant of angles relative to the adjacent ply fibers. The implications of the biaxial-bending are explored and discussed further in Section 3. Some secondary features that distinguish the biaxial-bending test from Canturri's work are the layups examined, the use of dynamic loads, and the progressive damage characterization that will be described in Section 2.3.

2.2. Test specimens

The CFRP test specimens were manufactured using an IM7/8552 carbon fiber-epoxy material system and cured according to the manufacturer's instructions [16]. Material properties for this material system can be found in Part II of this paper [14]. The specimen geometry and layups are described in Figure 3. Three layups were tested and the results are presented in this paper. The three layups selected were chosen so that migration could be studied through 90°, 45°, and -45° plies. Square plates (105 mm × 105 mm) were manufactured with a circular Polytetraflouroethylene (PTFE) insert (13 μm thick, 10 mm radius) located at the center point of the plate at the interface designated by "T" in Figure 3. The plates were then cut symmetrically about the center point to create four 52.5 mm × 52.5 mm square test specimens, each with a quarter circle PTFE insert in one corner. The cut specimens were then ultrasonically scanned to ensure that the insert placement was correct. The total cured specimen thickness was 6.12 mm.

The specimen geometry was selected as a relatively high length-thickness aspect ratio (i.e, shear deflection is *not* negligible) to ensure that the response behavior remained in the "small deflection" domain. The motivation for limiting the test to small deflections was so that the test data could be used to validate models that are also limited to this domain.

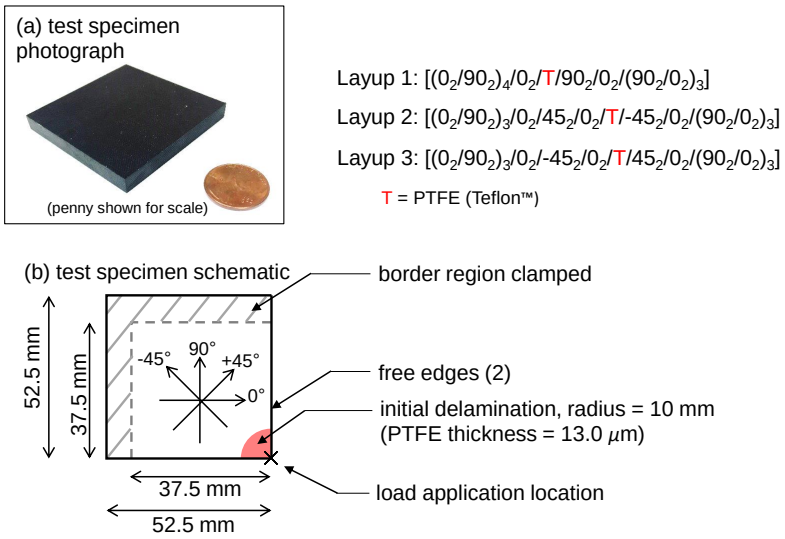

Figure 3: Biaxial-bending test specimen.

2.3. Quasi-static test setup

Quasi-static tests were performed at NASA Langley Research Center. The quasi-static test setup is shown in Figure 4. A square CFRP specimen was clamped in one corner of a steel picture-frame impact test fixture. Four bolts, one in each corner of the fixture, were each tightened to a torque of 5.64 N·m, resulting in a clamped condition that held the specimen firmly in the fixture, but was not so tight as to damage the specimens. Guide plates on the lower clamping surface, seen in Figure 4c, ensured that all specimens were in the same position when placed in the clamp. A 22.2 kN servo-hydraulic test frame was used to apply the quasi-static loads at a rate of 0.127 mm/min. Load was applied vertically to the free corner of the specimen using a 38 mm radius steel indenter tip.

Multiple quasi-static load cycles were carried out for each specimen, and ultrasonic testing (UT) and X-ray computed tomography (CT) scans were performed on the specimens after each load cycle so that damage could be documented progressively. The number of load cycles applied to a given specimen varied between one and eleven. In certain tests, several "pre-delamination" load/scan cycles were performed by applying a load below that of delamination

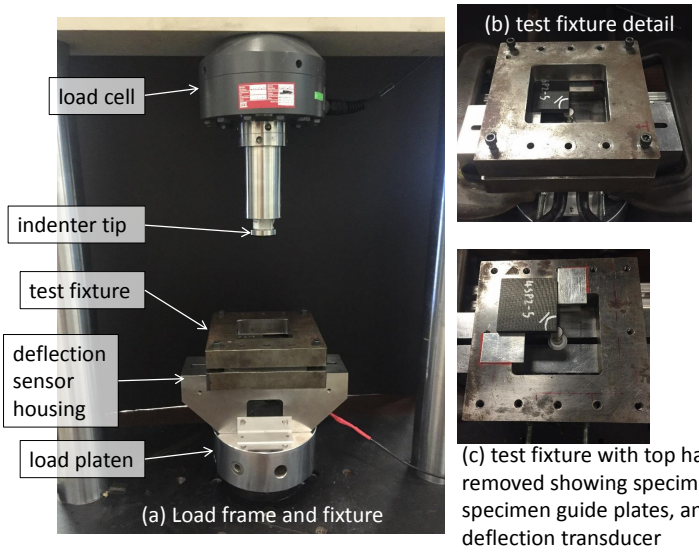

Figure 4: Quasi-static test setup.

initiation, to determine if any small amount of damage in any form was occurring prior to the observed delamination initiation. Test specimen deflection was measured from the specimen bottom surface using a mechanical transducer placed in a frame below the test fixture (see Figures 4b and 4c). The mechanical transducer was used to measure the true deflection of the specimen, absent any influence from test stand or fixture deformation.

2.4. Low-velocity impact test setup

Low-velocity impact tests were performed at Swerea SICOMP[4]. A steel picture frame impact test fixture was manufactured to replicate the quasi-static fixture. The impact test fixture had the same dimensions as the quasi-static fixture but was designed so that it could be integrated with the impact drop weight tower at SICOMP. A 38 mm radius steel impact tip was manufactured to replicate the quasi-static indenter tip, but as with the impact test fixture, the impact tip was manufactured to work with the existing equipment at SICOMP.

The impact test fixture is shown in Figure 5a. The test fixture was positioned

[4]Swedish composites research institute, http://www.swerea.se/sicomp

beneath an instrumented drop weight tower. The drop weight was equipped with a piezoelectric ring sensor (connected to a current source) to measure force during impact. The impact tip was attached to the end of the drop weight. The total mass of the drop weight assembly was 3.091 kg. The drop weight was raised by a rope to its desired drop height and released using an electromagnet at the end of the rope. Drop weight velocity just before impact was measured using a transmissive photo-microsensor that was attached to the guide tube. The photo-microsensor measured the passing time of a small steel tube attached to the drop weight just before impact so that the velocity may be determined. A laser distance sensor, accurate to 17.5 μm, was used to record the underside deflection of the specimen during impact. All the instrumentation was connected to a digital oscilloscope which recorded the signals during the impact events. The data were recorded and saved to a computer file for further processing.

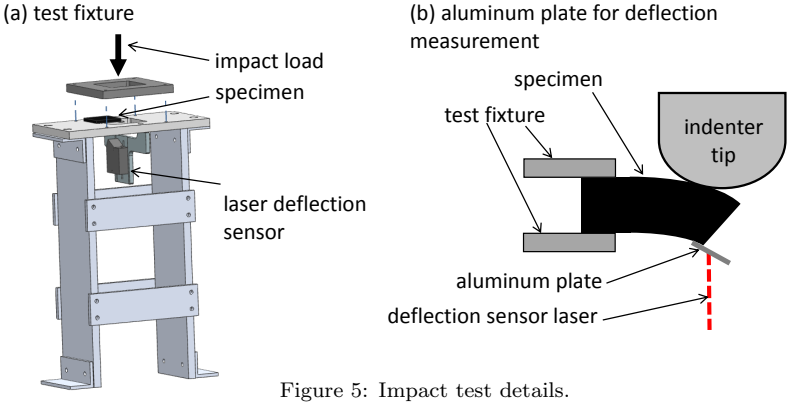

Figure 5: Impact test details.

Because the deflection was measured on the specimen corner, it was thought that there could be a risk that the specimen would deflect and rotate such that the laser measurement point would fall off of the bottom surface of the specimen and give an incorrect measurement. This is illustrated in Figure 5b. To mitigate this risk, small aluminum plates were bonded to the specimen lower surface at the corner to serve as a surface for the laser to obtain readings from, no matter the specimen rotation/deflection (see Figure 5b). Readings from the aluminum plate lead to data that very slightly overestimate the actual deflections; how-

ever, based on the small angle at the edge of the specimen, this overestimation was determined analytically to be less than 1% (the deflection in Figure 5b is exaggerated for illustrative purposes).

Each specimen was initially impacted at 2 J, which was the estimated impact energy required for delamination initiation, based on the critical force and displacement seen in the quasi-static tests. Since this energy was only an estimate, damage in each specimen was investigated after impact using a handheld ultrasound C-scanner with a resolution of approximately +/- 1 mm. Using the scanner, the size and shape of the delaminations could quickly be determined. If a specimen did not show any delaminations after the first impact load, the impact energy was raised slightly and the specimen was impacted again. This was repeated as many times as necessary until delamination was observed (see Section 4 for further discussion).

A small number of quasi-static tests were also performed at SICOMP to ensure that the fixture and impact tip were equivalent structurally to those used for the quasi-static tests performed at NASA. The test fixture and rigid base used in the impact tests were placed in an MTS testing machine that had the impact tip attached to the machine crosshead. The laser distance sensor was attached to the test fixture underneath the specimen, as in the impact test.

3. Quasi-static test results and discussion

Most of the specimens were tested with multiple load/unload cycles. Specimens are named according to number and the plate they were cut from (i.e., "XP3-1" refers to specimen 1 from cross-ply plate 3). The number of specimens tested for each layup is inconsistent due to errors in fabrication and, in the case of Layups 2 and 3, the position/orientation a particular specimen had in the plate it was cut from. Force-displacement data are plotted showing only the regions from each load cycle that do not overlap. This method of plotting is utilized to clarify the data presentation and is illustrated in Figure 6 where Specimen XP3-2 is used as an example. Force-displacement data for all tests

are shown in Figure 7. In Figure 7, the maximum forces for "pre-delamination" load cycles (as described in Section 2.3) are identified by points i through iv for each layup. The load cycles labeled using Arabic numbers correspond to ultrasonic scan images shown in Figures 8, 12, and 14. The force-displacement data from the quasi-static tests may be useful for numerical model development and validation purposes.

Some variance can be seen in the critical force required for delamination initiation for each layup. A post-mortem inspection revealed that the actual PTFE insert radii were generally less than 10 mm and varied between specimens by approximately +/- 1 mm. Because bending moment decreases with distance from the clamped edges, the specimens with smaller PTFE inserts had a relatively lower energy release rate for a given deflection level and therefore a higher critical force when delamination initiated. Better consistency between inserts geometry in the specimens was not possible using the manufacturing equipment available.

After the initial elastic response leading up to the critical force, the subsequent damage growth stability depended on how much strain energy had built up before initiation. In cases where the critical force was higher, initiation was followed first by unstable delamination growth, and then by continued stable growth. In cases where the critical force was lower, damage growth was stable throughout. Dashed portions of the curves are used in instances where, due to brief unstable growth and a resulting rapid deflection for a small amount of time, the deflection transducer lost contact with the specimen.

Further understanding of the observed damage can be gained from UT scans of a representative specimen from each layup. Generally, delamination grows radially in all directions from the insert; however, the interfaces and regions in the specimen where delaminations formed was different for the three layups tested. Layup 1 UT scans are shown in Figure 8a from the "top" (i.e., loaded) side of test specimen XP3-6 for loading conditions from "pre-delamination" load iv, just as delamination begins, through Load 7, after delamination initiation and migration. The bottom surfaces of the specimens were also scanned to confirm

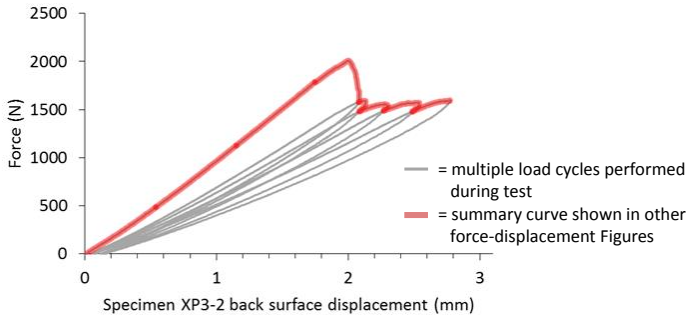

Figure 6: Multiple load cycles and summary force-displacement curve for specimen XP3-2.

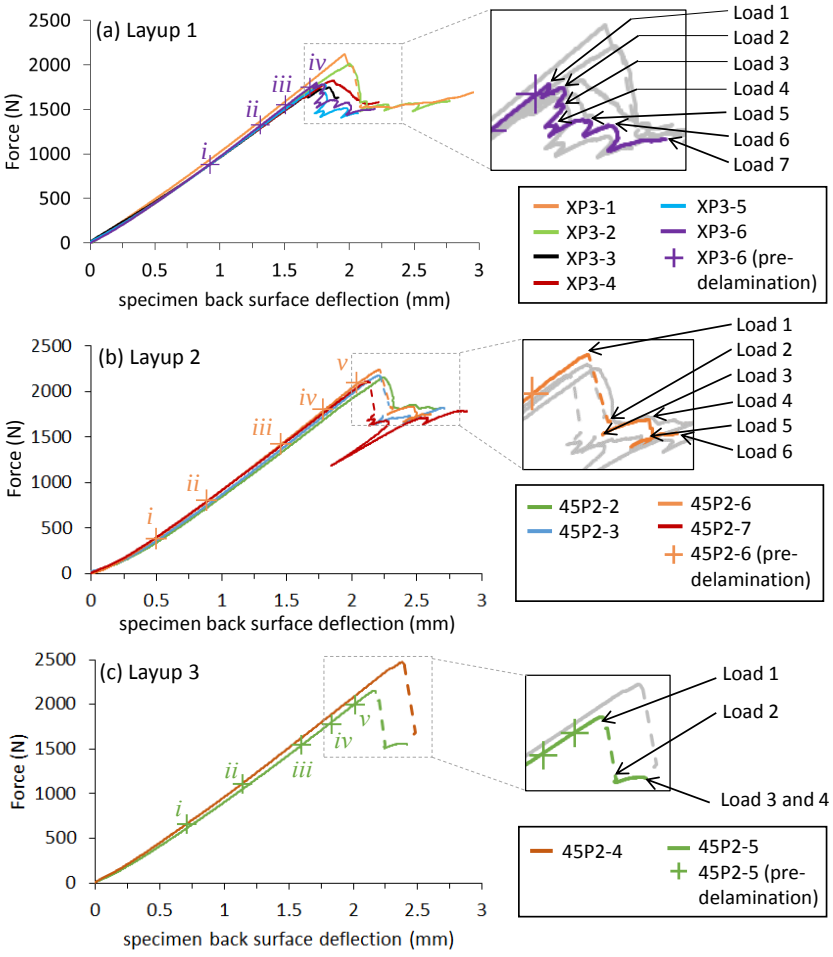

Figure 7: Quasi-static force-displacement data.

that no additional delaminations were present and were hidden in the shadow of those shown in the figure. The damage shown in Figure 8 is representative of damage seen in all of the Layup 1 specimens. Two delaminations grew during the test from the PTFE insert, at the two interfaces identified in Figure 8. The scan labeled "Load *iv*" shows the PTFE quarter-circle insert, as well as the first instance of delamination growth at the region above the PTFE boundary near the right hand side of the specimen.

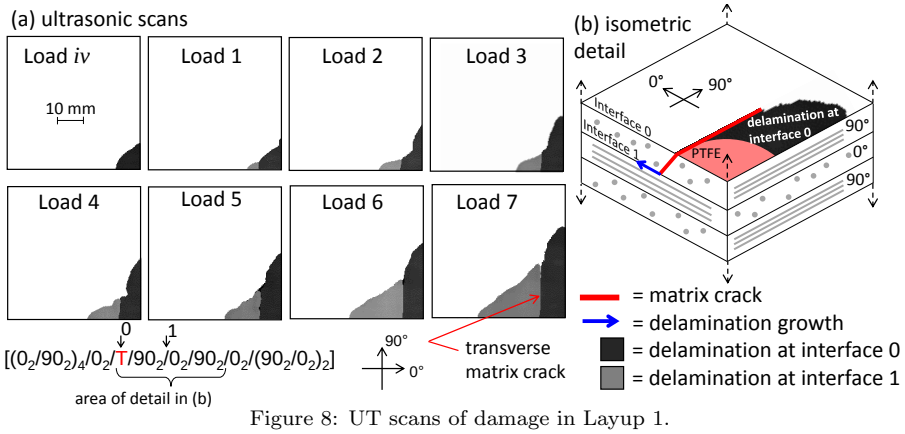

Figure 8: UT scans of damage in Layup 1.

In the region of the PTFE border near the lower edge of the specimen, the delamination migrated almost immediately down to interface 1 and then continued to grow at that interface, bounded below by 0° fibers. In the region of the PTFE near the right hand edge of the specimen, the delamination grew in the 90° direction and remained at that same interface (interface 0) bounded below by 90° fibers. The two delaminations share a boundary consisting of a transverse matrix crack through the 90° plies between interface 0 and interface 1, as shown in Figure 8. The transverse matrix crack began as the initial migration from the PTFE film. The transverse matrix cracking is illustrated in detail in Figure 8b.

The delamination-migration mechanism seen in these tests was studied by Ratcliffe et al. [13]. In their work, delamination-migration was explained by demonstrating that the sign of the in-plane shear stress at a delamination front dictates an out-of-plane directional growth tendency. As illustrated in Figure

9, the sign of the shear stress at a Mode II delamination front dictates the orientation about an in-plane axis of a series of Mode I microcracks in the resin rich region between the delaminating plies. If the microcracks are oriented to guide the delamination towards fibers that have an orientation that arrests their growth (that is, further growth of the microcracks would require breaking fibers), they will coalesce into a macrocrack, be redirected along the bounding fiber direction, and form a delamination. An example is shown in Figure 9a for a simple [0/90/0] laminate. If the microcracks are oriented to guide the delamination such that it is not contained by bounding fibers, they still may coalesce, but instead of forming a delamination, they form a transverse matrix crack that grows in between fibers through a ply. After formation of the transverse crack, the delamination may resume at a new interface once a new fiber orientation is reached that arrests the transverse growth, as shown in Figure 9b.

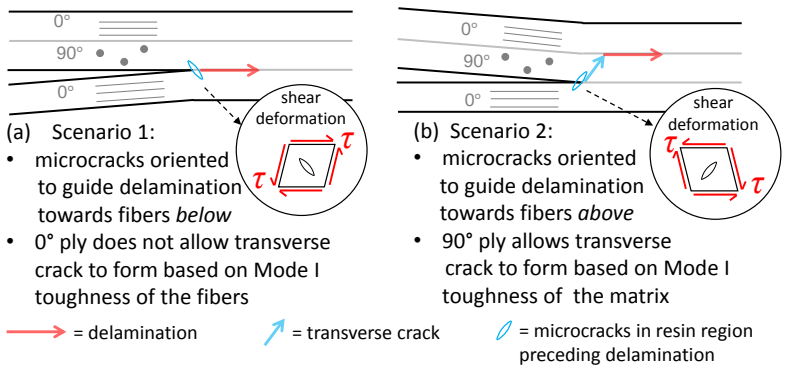

Figure 9: Illustration of delamination migration in a [0/90/0] layup.

In the biaxial-bending specimens, the deformation and resulting shear stress sign are such that the microcracks are always guiding delaminations towards the ply below. Additionally, past observations suggest that the microcrack orientation about an in-plane axis is a function of the G_I/G_{II} ratio [17] and microcrack orientation about the laminate normal axis is a function of the G_{II}/G_{III} ratio [18]. Specifically, microcrack orientation about the laminate normal axis was seen to be perpendicular to the direction of delamination growth for pure Mode II delamination. One interpretation of these observations (though not explic-

itly proven) is that microcrack orientation about the laminate normal axis is perpendicular to the direction of maximum energy release rate.

The biaxial-bending tests are designed so that, under the indentation loading, the moment orientation varies smoothly across the PTFE insert boundary from pure M_x at one free edge to pure M_y at the other free edge where x and y are orthogonal in-plane axes aligned with the specimen edges. Based on this moment distribution, the following conclusions can be made: (1) the direction of maximum energy release rate (pure Mode II) varies smoothly along the entire PTFE insert boundary spanning all possible angles, α, relative to the bounding fibers in the ply below, and (2) the direction of ply shearing follows the same smooth variation along the PTFE insert boundary and therefore, in the case of this specimen, is oriented approximately the same as the direction of maximum in plane shear energy release rate.

Microcrack orientation about the out-of-plane axis, and ply shearing vectors are illustrated in Figure 10a, where $0^\circ \leq \alpha \leq 90^\circ$ and microcracks are illustrated (in plan view) by dashed red lines. In the region of the PTFE boundary near the lower edge of the specimen, where the ply shearing vector is perpendicular to the 90° fibers below, the microcrack orientation is perpendicular to the ply shearing direction and parallel to the 90° bounding fibers. Therefore, in this case, the microcracks propagated easily through the 90° plies in the form of a matrix crack, and the delamination migrated to interface 1. In the region of the PTFE near the right hand side of the specimen, however, the ply shearing direction is in line with the 90° bounding fibers and the microcrack growth direction is perpendicular to the bounding fibers. As a result, the microcracks cannot coalesce and grow through the ply as a matrix crack and instead coalesce at interface 0 as delamination growth occurs.

Finally, for ply shearing directions that are in between perpendicular and parallel to bounding fibers, there was a certain range of α where several transverse cracks formed and migration began; however, only the first transverse crack to form actually completed the migration process and led to continued delamination on the new interface. This can be seen in the CT scans shown in

Figures 10b and 10c. A distinction is observed here between "migration" and simply formation of a transverse matrix crack branching off of a delamination. More investigation is warranted on understanding the occurrence of migration for delamination growth directions that are neither parallel nor perpendicular to bounding fibers.

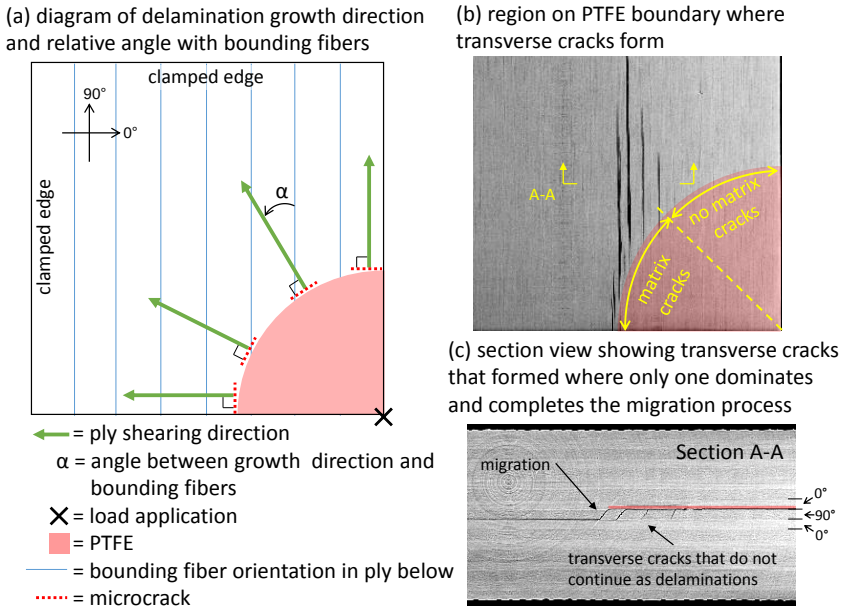

Figure 10: Delamination growth and migration detail (CT images from specimen XP3-6).

A final observation regarding migration is that the first transverse matrix crack (i.e., the one that ultimately led to migration) was seen to form at "pre-delamination" load i in specimen XP3-6, well before the initiation of delamination growth. Computed tomography (CT) images are shown in Figures 11b–d that were captured at "pre-delamination" points along the load curve, as identified in Figure 11a, for specimen XP3-6. This matrix cracking is not evident from a simple inspection of the force-displacement curve, which indicates that the energy required to form this crack is very small and possibly negligible in the context of the global damage process. This same observation regarding the energetic insignificance of matrix cracking in these type of progressive damage process (i.e., delamination dominated) was made previously by McElroy et al.

[19].

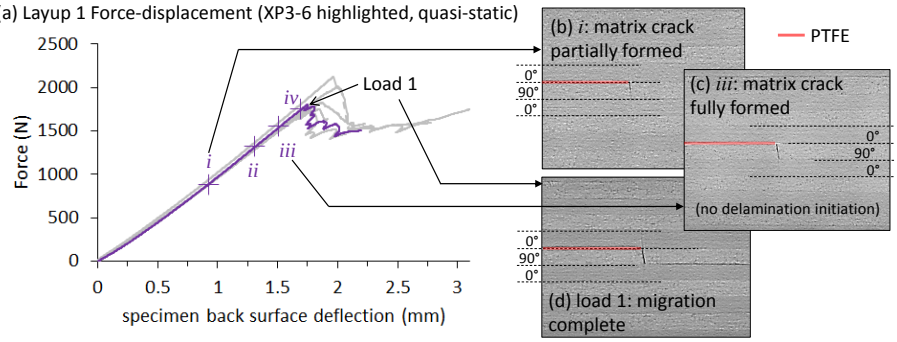

Figure 11: CT images of transverse matrix cracks forming incrementally before delamination growth initiation (specimen XP3-6).

Layup 2 UT scans are shown in Figure 12a from the "top" (i.e., loaded) side of specimen 45P2-6, which underwent six load cycles after the "pre-delamination" loads. The damage shown is representative of damage seen in all of the Layup 2 specimens. Delaminations grew during the test from the PTFE insert at the three interfaces defined in Figure 12. In this layup, delamination emanating from the central region of the PTFE boundary remained at interface 0 and was bounded by the -45° fibers below. In the region of the PTFE boundary near the lower edge of the specimen, the delamination migrated through the -45° plies and then continued growth in interface 1, bounded by 0° fibers below. In the region of the PTFE boundary near the right hand side of the specimen, the delamination migrated through both the -45° and 0° ply groups and then continued growth at interface 2, bounded by 90° fibers below. The transverse matrix cracking is illustrated in detail in Figure 12b. Additionally, in this region, as seen in Figure 12 at Load 3, the delamination at interface 0 has grown such that it obscures the already existing delamination below, at interface 2.

The delaminations at interface 1 and interface 0 share a boundary consisting of a transverse matrix crack in the -45° plies. The boundary that the delamination at interface 0 shares with that of interface 2 is more complex. From interface 0, a transverse matrix crack extends down through the -45° fibers to interface 1 ("0-1 crack"). For this crack to proceed further on the same path

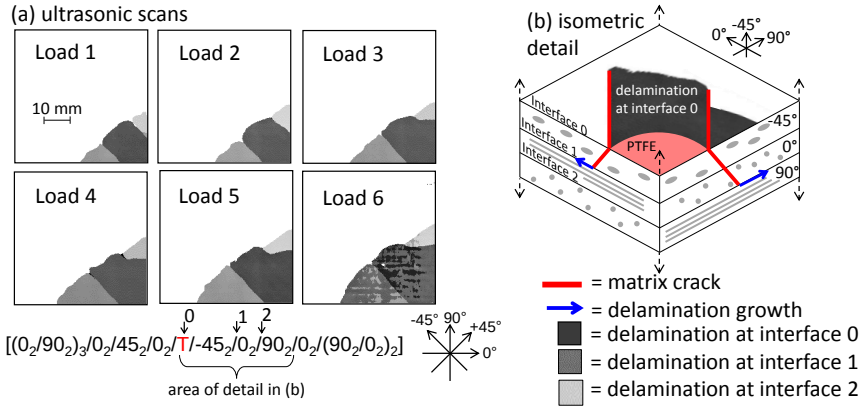

Figure 12: UT scans of damage in Layup 2.

through the thickness down to interface 2, fibers would have to be broken, which did not occur. Instead, a series of smaller disconnected transverse matrix cracks through the 0° ply below interface 1 formed along the path of the 0-1 crack. This is shown in the CT images in Figure 13. The damage pattern seen in the Layup 2 specimens is thought to be particularly useful for progressive damage model development and validation, as it contains two types of interactions between delaminations that can occur during LVI: (1) a simple matrix crack through fibers of the same orientation and (2) a "staggered migration" consisting of a system of matrix cracks in different layers and at different orientations, but following the same global path through the specimen. These two mechanisms were not compared and quantified in terms of dissipated energy.

Layup 3 UT scans are shown in Figure 14 from the "top" (i.e., loaded) side of specimen 45P2-5, which underwent four load cycles after the "pre-delamination" loads. The damage shown is representative of damage seen in both of the Layup 3 specimens. Delaminations grew during the test from the PTFE insert at interfaces 1 and 2, as shown in in Figure 14. In the region of the specimen near the lower edge, migration occurred through the 45° plies via a transverse matrix crack that was arrested by fibers in the 0° ply. A delamination continued from this location on interface 1. In the region of the specimen near the right hand side of the specimen, staggered migration occurred via multiple matrix cracks

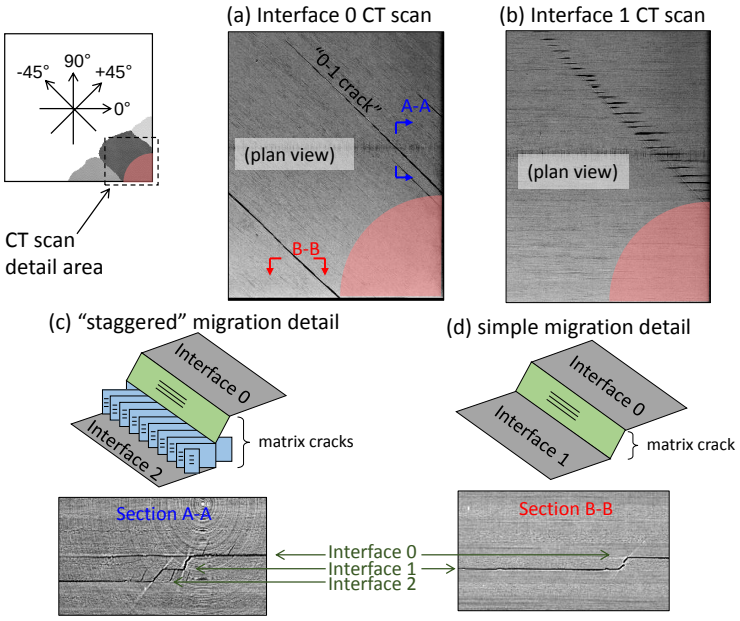

Figure 13: CT scans showing "staggered" and simple migration in Layup 2.

through two ply blocks of differing fiber orientation. The staggered migration here consists of a transverse matrix crack oriented along the 45° fibers extending down to interface 1. Below this crack are transverse matrix cracks running parallel to the 0° fibers extending down to interface 2. Delamination growth continued from here at interface 2. Connecting the delaminations at Interfaces 1 and 2 is a transverse matrix crack. The transverse matrix cracking is illustrated in detail in Figure 14b.

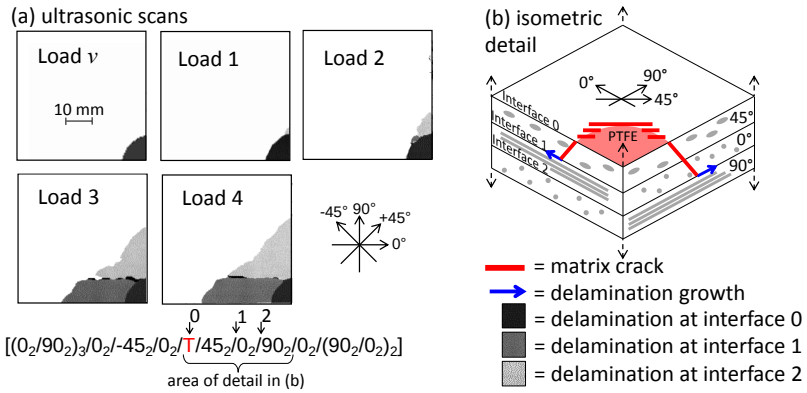

Figure 14: UT scans of damage in Layup 3.

A particular advantage of the cyclic load/scan test procedure is the ability to observe and record damage at multiple intermediate stages of growth. These types of data are useful in progressive damage model development and validation, as they provide experimental reference points throughout an entire analysis, rather than just at the final state of damage. Delamination area has been used previously as a metric to study in progressive damage testing and analysis [20, 21]. Figure 15 shows the area of delaminations versus the deflection of the specimen back surface observed in the quasi-static biaxial-bending tests. The delamination area data are meant to augment the force-displacement data in terms of numerical model validation, where, for a general progressive damage model, neither data set alone is sufficient for complete model validation.

In Figure 15, $A^{(tot)}$ refers to the summation of the areas of all delaminations at all interfaces, and $A^{(0)}$, $A^{(1)}$, and $A^{(2)}$ refer to the delamination area at interface 0, interface 1, and interface 2, respectively. For each layup, data from all specimens tested are included. Polynomials are fit to each delamination growth data set and are shown so that they may be used for numerical model development and validation.

4. Low-velocity impact test results and discussion

Low velocity impact force-displacement data for all layups are shown in Figures 16a-16c. As in the quasi-static tests, all specimens experience an initial linear elastic response followed by a non-linear response caused by damage. Findings discussed in Section 3 and illustrated in Figure 11 show that transverse matrix cracks form at loads well below delamination initiation. Therefore, one may assume that, in cases where it was necessary to perform multiple impacts of increasing energy on one specimen in order to see delamination initiate, transverse matrix cracks were present after the first impact. However, these matrix cracks, while part of the overall damage initiation process, are energetically insignificant (according to observations in Figure 11) and would not affect the observed delamination process any differently than in the quasi-static tests.

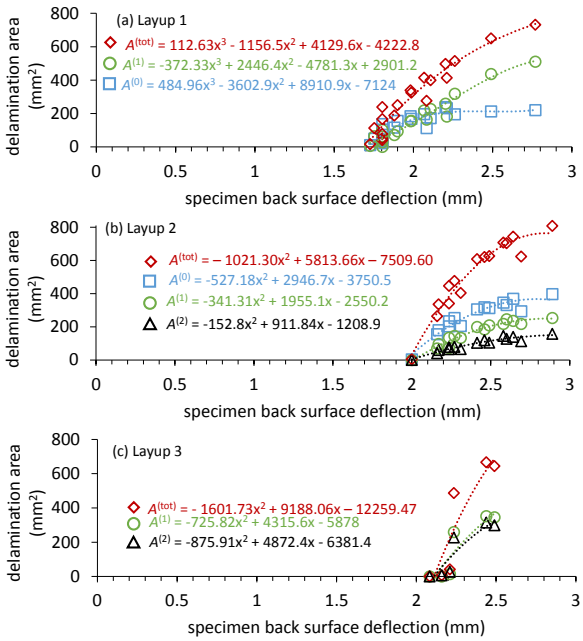

Figure 15: Delamination area versus specimen deflection for all quasi-static tests.

Representative UT scans for each layup showing delaminations resulting from impact are shown in Figure 17 and compared to their quasi-static counterparts. The damage patterns seen in Figure 17 for each layup correspond well with the quasi-static tests as, for each layup, the same damage path is followed. The only exception to this observation is in Layup 2 where the delamination at interface 0 grew above the delamination at interface 1 in the quasi-static test. This did not occur in the impact test. A physical description of the damage in each layup resulting from the impact loads would be redundant and the reader is referred back to Section 3.

Another correlation between the impact tests and the quasi-static tests can be made using the required energy to initiate delamination. In the impact tests, the initiation energy corresponds to the measured kinetic energy of the drop weight assembly just before the moment of impact. In the quasi-static tests, the initiation energy corresponds to the work (i.e., the integral of the force-displacement curve) up to the maximum load. Figure 18 shows a comparison of the average energy required for delamination initiation in each layup for

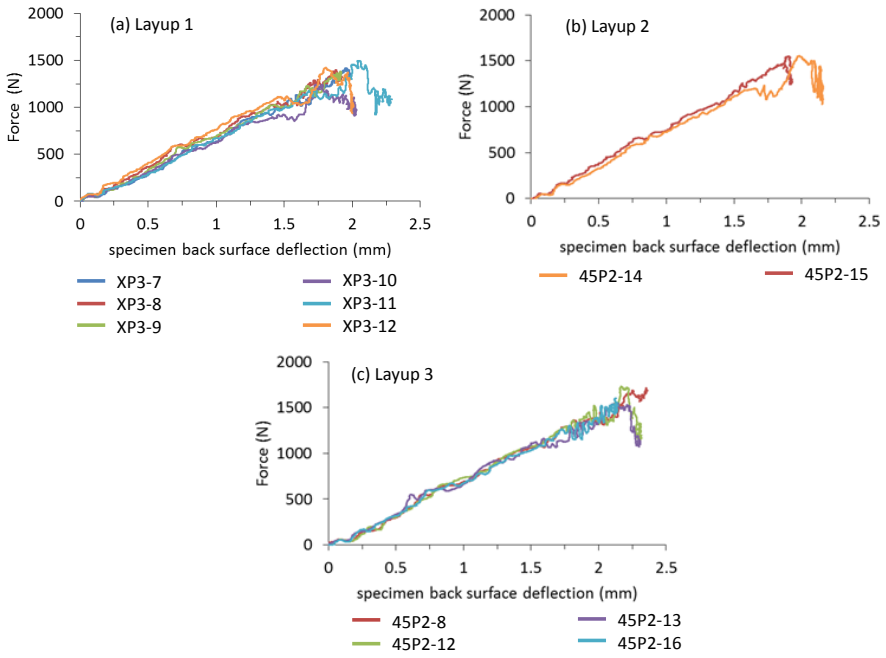

Figure 16: Low-velocity impact force-displacement data.

the quasi-static and impact tests. Data scatter, illustrated on each bar, either aligned closely or overlapped between the quasi-static and impact tests.

Figure 18 also shows that there is a difference in kinetic energy required to initiate damage for each layup. Olsson et al. observed that the Mode II toughness value, G_{IIc}, for delamination *initiation* from a thin insert (i.e., not for subsequent growth) was significantly higher for interface orientations of $0°/0°$ and $0°/5°$ than in an interface orientation of $0°/90°$ [22]. Similar differences in initial toughness were obtained in Mode II dominated buckling tests. The difference in initial toughness seems to be explained by the fact that the initial crack growth in the $0°/0°$ and $0°/5°$ interfaces occurred through a resin pocket ahead of the film insert, while crack growth for $0°/90°$ interfaces initially occurred via a transverse matrix crack in the $90°$ ply, generating a sharp natural crack tip for the subsequent delamination growth. In these tests, the toughness in delamination growth after initiation was essentially independent of interface angle. Olsson's observations provide a possible explanation for the differing de-

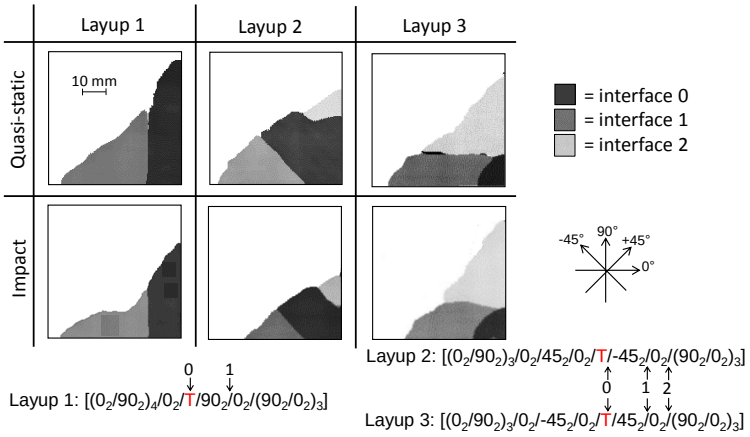

Figure 17: Representative UT scans of damage in impact and quasi-static tests.

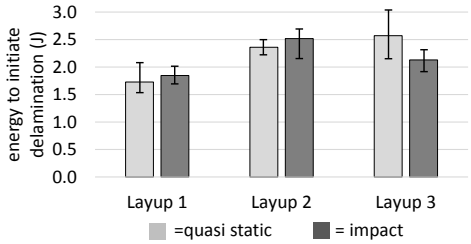

Figure 18: Energy required for initiation of delamination in the quasi-static and impact tests.

lamination initiation energies seen here, where the 0°/90° interface specimens (Layup 1) also were seen to have the lowest initiation energy.

Olsson et al.'s conclusions are supported by work by O'Brien et al., in which measured G_{IIc} for Mode II delaminations starting from a thin insert, effectively increased by an average factor of 1.59 due to a resin pocket that forms at the insert boundary [23]. In Section 3, matrix cracks were shown to form in the Layup 1 quasi-static test well before delamination initiation. The "pre-delamination" matrix crack formation occurred in Layup 3 to a limited extent near one edge only, and did not occur at all in Layup 2. The "pre-delamination" cracks in the biaxial-bending tests formed as Mode I cracks, thereby avoiding the Mode II toughness increase, and acted as "sharp" starter cracks for the delaminations that followed.

A comparison between representative quasi-static and impact force-displacement data is shown in Figure 19. The recorded impact force is lower than that of the

quasi-static indentation. This was somewhat surprising, as others previously have identified an approximate equivalence in structural response between quasi-static indentation and low-velocity/large-mass impact [24, 25, 26]. To investigate further, an impact test was performed at NASA, using a different impact load cell and using the quasi-static test fixture. Additionally, a quasi-static test was performed at SICOMP, using the impact test fixture. Figure 19 is plot of force-displacement data for Layup 1 from (1) quasi-static tests (orange), (2) LVI tests (red), (3) LVI tests using a different impact load cell and the quasi-static fixture (blue), and (4) quasi-static tests using the impact fixture (green).

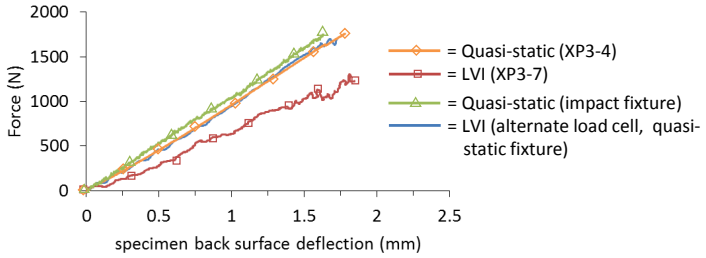

Figure 19: Investigation on error in force-displacement data from impact tests.

Several observations can be made from Figure 19. First, the recorded response between the quasi-static test (orange) and the impact test using the alternate load cell and quasi-static test fixture (blue) is essentially the same. Second, there is a difference in observed stiffness between results from tests performed using the impact test fixture (green) and tests performed using the quasi-static test fixture (blue), but this difference is small and presumably should not have a significant effect on the test results. Third, the impact force (red) is significantly lower than that of all three other tests, indicating that the load cell may have some inherent sensitivity or calibration issue.

With this information, a brief inspection of the impact test load cell was performed. An impact hammer containing a built in load cell was used to hit the load cell used in the impact tests. Data are shown in Figure 20, where the maximum force readings obtained from the hammer and impact test load cell are plotted versus one another. Equivalent readings from each source were only obtained if care was taken to center the hammer strikes on the impact test load

cell. The biaxial-bending test does not have a symmetric loading condition on the impact tip and therefore may introduce some small amount of bending into the drop weight–load cell assembly. This small eccentricity on the impact load cell may explain the lower force data.

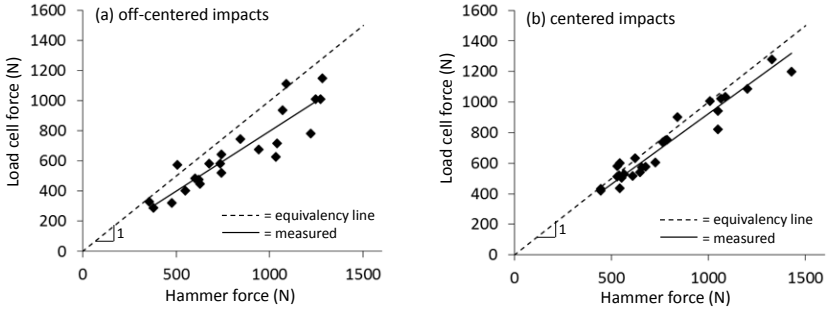

Figure 20: Measured forces from hammer and impact test load cells for centered and off centered load conditions. Data points are fit with a solid linear trendline to aid in comparison with the dashed line.

The damage patterns seen in the impact tests were qualitatively the same as those seen in the quasi-static tests. The required energy to initiate delamination also compared closely between the quasi-static and impact tests. Additionally, the data shown in Figure 19 indicate that the specimen force-displacement response in the impact tests that used the alternate load cell (i.e., the load cell not sensitive to eccentric loading) is equivalent to that of the quasi-static tests. Unlike the quasi-static tests, it is not advisable to use the raw force data from the impact tests for numerical LVI model validation purposes; however, there is evidence that the damage resulting from each type of load is either very similar or, as in most cases, equivalent.

5. Fracture surface microscopy

Six biaxial-bending specimens (one of each layup from quasi-static and impact loads) were selected to gather microscopy images from the fracture surfaces using a scanning electron microscope (SEM). The prominent microscale feature caused by Mode II delamination is the formation of cusps (also known as hackles) [17]. Figure 21 shows representative fracture surface images from several

locations in each layup. The assumed ply shearing direction is determined based on discussion in Section 3. Though the shearing direction in Figure 21c is approximately -45° for each layup, there is a small variation in angle due to the images having been taken from slightly different locations. Shear cusps are the dominant micro-scale damage feature observed throughout all of the specimens.

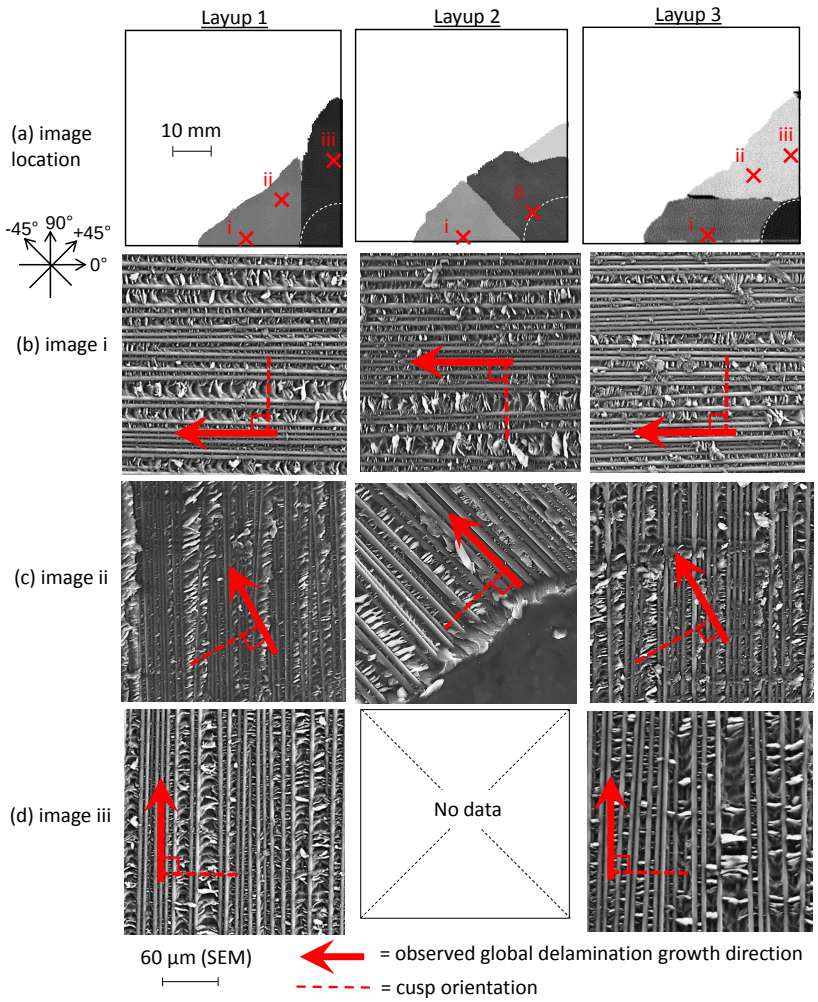

Figure 21: SEM images showing cusp orientation.

Following the discussion in Section 3, at a common location in the specimen, the orientation of cusps about a normal laminate axis shown in Figure 21 generally aligns with the orientation of the microcracks illustrated in Figure 10 where

the direction of assumed ply shearing is shown. This observation confirms findings in previous research where cusp orientation was seen to be influenced by the G_{II}/G_{III} ratio [18] and extends these findings by indicating that cusp orientation is perpendicular to the direction of maximum energy release rate. Care should be taken in interpretation of the relationship between cusp orientation and global delamination behavior, as in many instances cusps were observed to rotate and appear to be influenced by the presence and spacing of nearby fibers.

Another observation from the SEM images, potentially relevant for progressive damage model development, concerns the transverse matrix cracks. The fracture surface of a representative transverse matrix crack is shown in Figure 22. Cusps are visible between fibers on this crack surface, indicating that the transverse matrix crack propagates not from "top-to-bottom" in the transverse direction, but rather in the same manner as a delamination bound by fibers on the transverse crack surface. This information may be useful in developing a numerical model that captures this mechanism.

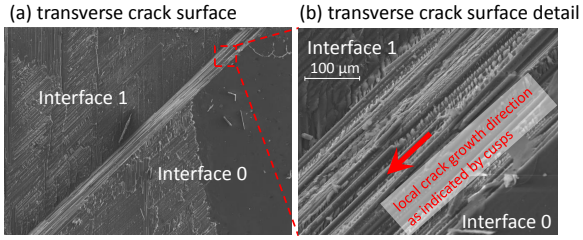

Figure 22: SEM images showing transverse matrix crack face (Layup 2).

6. Conclusion

A new test was presented that can create damage similar to that which occurs as a result of low-velocity impact on a composite laminate. The experimental data is intended to be used in numerical model development and validation. The test consists of a square carbon fiber reinforced polymer specimen that is subjected to a biaxial-bending state of deformation. By design, damage in the specimens consisted of no more than three delaminations at different interfaces interacting with one another via transverse matrix cracks.

Quasi-static tests generated specific data that may be used for validation of progressive damage models. This data includes force-displacement response, delamination area as a function of indentation, and a qualitative understanding of the damage mechanisms. Impact tests also generated data useful for model validation, including the required kinetic energy for delamination initiation and, again, a qualitative understanding of the damage mechanisms. The damage patterns seen in the impact tests matched those of the quasi-static tests. There also was good correlation between the required energy to initiate delamination in the impact tests and the required work to initiate delamination in the quasi-static tests. Overall, it was shown that the specimen response in the impact test is equivalent to that of the quasi-static tests.

Images of the fracture surfaces of several specimens were gathered using a scanning electron microscope. Cusps, caused by the Mode II delamination growth, were, in general, seen to be oriented about the transverse axis in alignment with the ply shearing direction. Finally, cusps were also seen on the transverse matrix cracks, indicating that these cracks do not grow "top-to-bottom" as in a migration, but rather they grow "sideways" along fibers in the same manner as a delamination.

7. Acknowledgments

The research was funded by and performed at NASA Langley Research Center and Swerea SICOMP. The authors would like to thank Dr. Renaud Gutkin, Dr. T. Kevin O'Brien, and Dr. James Ratcliffe for their advice and consultation concerning this body of work.

References

[1] Building block approach for composite structures, in: Composite Materials Handbook (Volume 3, Chapter 4) CMH-17, Wichita State University, National Institute for Aviation Research, 2012.

[2] P. Feraboli, Composite materials strength determination within the current certification methodology for aircraft structures, Journal of Aircraft 46 (4) (2009) 1365–1374.

[3] J. Allison, Integrated computational materials engineering: A perspective on progress and future steps, JOM: The Journal of the Minerals, Metals and Materials Society 63 (4) (2011) 15.

[4] J. Allison, D. Backman, L. Christodoulou, Integrated computational materials engineering: a new paradigm for the global materials profession, JOM: The Journal of the Minerals, Metals and Materials Society 58 (11) (2006) 25–27.

[5] D. Apelian, Integrated computational materials engineering (ICME): A model for the future?, JOM: Journal of the Minerals, Metals and Materials Society 60 (7) (2008) 9–10.

[6] C. Rose, C. Dávila, F. Leone, Analysis methods for progressive damage of composite structures, NASA/TM 2013-218024, NASA, 2013.

[7] P. Liu, J. Zheng, Recent developments on damage modeling and finite element analysis for composite laminates: A review, Materials & Design 31 (8) (2010) 3825–3834.

[8] ASTM D5528-01 Standard test method for mode I interlaminar fracture toughness of unidirectional fiber-reinforced polymer matrix composites, in: 2004 Annual Book of Standards, Vol. 15.03, ASTM International, West Conshohoken, PA (USA), 2004.

[9] ASTM D7905 Standard test method for determination of the mode II interlaminar fracture toughness of unidirectional fiber-reinforced polymer matrix composites, in: 2014 Annual Book of ASTM Standards, Vol. 15.03, ASTM International, West Conshohoken, PA (USA), 2014.

[10] ASTM D6671M-04 Standard test method for mixed modeI-mode II interlaminar fracture toughness of unidirectional fiber-reinforced polymer ma-

trix composites, in: 2004 Annual Book of Standards, Vol. 15.03, ASTM International, West Conshohoken, PA (USA), 2004.

[11] I. Paris, P. Minguet, T. O'Brien, Comparison of delamination characterization for IM7/8552 composite woven and tape laminates, in: Composite Materials: Testing and Design, Fourteenth Volume, ASTM International, 2003.

[12] P. Hansen, R. Martin, DCB, 4ENF and MMB delamination characterisation of S2/8552 and IM7/8552, Tech. rep. (1999).

[13] J. Ratcliffe, M. Czabaj, T. O'Brien, A test for characterizing delamination migration in carbon/epoxy tape laminates, NASA/TM-2013-218028, NASA, 2013.

[14] M. McElroy, R. Gutkin, M. Pankow, Interaction of delaminations and matrix cracks in a CFRP plate, Part II: Simulation using an enriched shell finite element model (submitted), Composites Part A: Applied Science and Manufacturing.

[15] C. Canturri, E. Greenhalgh, S. Pinho, J. Ankersen, Delamination growth directionality and the subsequent migration processes–the key to damage tolerant design, Composites Part A: Applied Science and Manufacturing 54 (2013) 79–87.

[16] Hexcel, Hexply 8552 Epoxy Matrix, product data (http://www.hexcel.com/Resources/), Hexcel, 2013.

[17] E. Greenhalgh, C. Rogers, P. Robinson, Fractographic observations on delamination growth and the subsequent migration through the laminate, Composites Science and Technology 69 (14) (2009) 2345–2351.

[18] C. Canturri, E. Greenhalgh, S. Pinho, The relationship between mixed-mode II/III delamination and delamination migration in composite laminates, Composites Science and Technology 105 (2014) 102–109.

[19] M. McElroy, F. Leone, J. Ratcliffe, M. Czabaj, F. Yuan, Simulation of delamination–migration and core crushing in a CFRP sandwich structure, Composites Part A: Applied Science and Manufacturing 79 (2015) 192–202.

[20] H. Suemasu, O. Majima, Multiple delaminations and their severity in circular axisymmetric plates subjected to transverse loading, Journal of Composite Materials 30 (4) (1996) 441–453.

[21] V. Lopresto, G. Caprino, Damage mechanisms and energy absorption in composite laminates under low velocity impact loads, in: Dynamic Failure of Composite and Sandwich Structures, Springer, 2013, pp. 209–289.

[22] R. Olsson, J. Thesken, F. Brandt, N. Jonsson, S. Nilsson, Investigations of delamination criticality and the transferability of growth criteria, Composite Structures 36 (1997) 221–247.

[23] T. O'Brien, W. Johnston, G. Toland, Mode II interlaminar fracture toughness and fatigue characterization of a graphite epoxy composite material, NASA/TM 2010-216838, NASA, 2010.

[24] P. Sjoblom, J. Hartness, T. Cordell, On low-velocity impact testing of composite materials, Journal of Composite Materials 22 (1) (1988) 30–52.

[25] W. Jackson, C. Poe, The use of impact force as a scale parameter for the impact response of composite laminates, Journal of Composites Technology and Research 15 (1993) 282–282.

[26] I. Choi, C. Hong, New approach for simple prediction of impact force history on composite laminates, AIAA Journal 32 (10) (1994) 2067–2072.